

EllSeg-Gen, towards Domain Generalization for head-mounted eyetracking

RAKSHIT S. KOTHARI*, Rochester Institute of Technology, USA

REYNOLD J. BAILEY, Rochester Institute of Technology, USA

CHRISTOPHER KANAN, Rochester Institute of Technology, USA

JEFF B. PELZ, Rochester Institute of Technology, USA

GABRIEL J. DIAZ, Rochester Institute of Technology, USA

The study of human gaze behavior in natural contexts requires algorithms for gaze estimation that are robust to a wide range of imaging conditions. However, algorithms often fail to identify features such as the iris and pupil centroid in the presence of reflective artifacts and occlusions. Previous work has shown that convolutional networks excel at extracting gaze features despite the presence of such artifacts. However, these networks often perform poorly on data unseen during training. This work follows the intuition that jointly training a convolutional network with multiple datasets learns a generalized representation of eye parts. We compare the performance of a single model trained with multiple datasets against a pool of models trained on individual datasets. Results indicate that models tested on datasets in which eye images exhibit higher appearance variability benefit from multiset training. In contrast, dataset-specific models generalize better onto eye images with lower appearance variability.

CCS Concepts: • **Computing methodologies** → **Image segmentation**; **Machine learning**.

Additional Key Words and Phrases: Domain Generalization, Semantic Segmentation

ACM Reference Format:

Rakshit S. Kothari, Reynold J. Bailey, Christopher Kanan, Jeff B. Pelz, and Gabriel J. Diaz. 2022. EllSeg-Gen, towards Domain Generalization for head-mounted eyetracking. *Proc. ACM Hum.-Comput. Interact.* 6, ETRA, Article 139 (May 2022), 27 pages. <https://doi.org/10.1145/3530880>

1 INTRODUCTION

Eye tracking solutions frequently employ computer vision or machine learning (ML) algorithms to extract features of interest from images captured using eye cameras. These features facilitate the estimation of a subject's gaze position. While numerous efforts have explored both approaches, recent works [4, 11, 15, 26, 32, 60, 64] report that ML systems demonstrate state of the art performance in identifying gaze relevant features for head-mounted eyetracking. Contrary to computer vision approaches where features are identified using handcrafted algorithms and heuristics, superior performance by ML is partly achieved by making minor adjustments in a ML system's internal parameters with the objective to maximize the probability of predicting known outputs for given training inputs [59]. A ML system with millions of parameters could theoretically demonstrate

Authors' addresses: Rakshit S. Kothari, rsk3900@rit.edu, rsk3900@rit.edu, Rochester Institute of Technology, 1 Lomb Memorial Drive, Rochester, NY, USA, 14623; Reynold J. Bailey, Rochester Institute of Technology, 1 Lomb Memorial Drive, Rochester, NY, USA, 14623; Christopher Kanan, Rochester Institute of Technology, 1 Lomb Memorial Drive, Rochester, NY, USA, 14623; Jeff B. Pelz, Rochester Institute of Technology, 1 Lomb Memorial Drive, Rochester, NY, USA, 14623; Gabriel J. Diaz, Rochester Institute of Technology, 1 Lomb Memorial Drive, Rochester, NY, USA, 14623.

Permission to make digital or hard copies of all or part of this work for personal or classroom use is granted without fee provided that copies are not made or distributed for profit or commercial advantage and that copies bear this notice and the full citation on the first page. Copyrights for components of this work owned by others than ACM must be honored. Abstracting with credit is permitted. To copy otherwise, or republish, to post on servers or to redistribute to lists, requires prior specific permission and/or a fee. Request permissions from permissions@acm.org.

© 2022 Association for Computing Machinery.

2573-0142/2022/5-ART139 \$15.00

<https://doi.org/10.1145/3530880>

perfect performance over the distribution of data it was trained on. These systems however often fail to generalize to out-of-distribution samples that are dissimilar to ones seen during training but plausible under the overarching goals of the problem. For example, ML systems trained to segment eye images acquired with a small subset of the human population, or optimized for particular imaging hardware, may fail to generalize onto the average use case.

In the context of eyetracking, high performance across subjects, environmental reflection, camera quality, camera placement and eye occluding artifacts can be cast as a Domain Generalization problem [2, 36, 39, 54]. Although the intuitive thought is that a broader training set will always produce the most generalizable model, it may come at the cost of performance [45, 63, 65] as a significantly broader distribution must be captured by limited network complexity [38]. A relevant and alternative approach to solving the generalization problem would be to assemble a suite of domain-specific models. These specialized models theoretically have attained the ceiling performance on a domain while remaining agnostic to others. At run-time, one could select a model trained on a domain that maximizes statistical similarity to the intended testing data. The notable drawback to this approach is that it assumes the existence of a hypothetical method which finds the best matching model without any test-time labels or annotations (for example, one may consider model uncertainty [29] as a measure of performance). Figure 1 is a graphical example to illustrate these approaches one may adopt for optimal generalization.

Collecting and annotating data is a difficult and time consuming task. In context to head-mounted eyetracking, we often collect and annotate a small subset of data drawn from a few users with the hope that our model would generalize to a broader population. Models trained on a biased sampling of the intended distribution may not generalize well beyond a few subjects or gaze positions [40]. For example, a model trained on eye images with a narrow gaze distribution or specific eye camera orientation may not generalize to users with non-overlapping or broader gaze distribution and camera orientation. We hypothesize that jointly training with multiple datasets may expand the available training distribution and in turn improve generalization across data collected from different subjects under the same environmental conditions.

In this work, we explore the relationship between model generalizability and performance within the context of eye tracking. The specific contributions of this work are as follows:

- We test the hypothesis that a single model trained on data drawn from multiple heterogeneous domains can generalize better than a specialized, dataset-specific model when evaluated on domains **unseen during training**. If we accept this hypothesis, then it suggests there is a benefit in expanding the breadth of the training distribution by accumulating more data. If we reject this hypothesis, then the better approach to achieve generalizability is by exploring test-time techniques to find the optimal model from a pool of dataset-specific models.
- A model may not generalize well across subjects due to a distribution shift caused from a limited or biased sampling of the data distribution. We hypothesize that training with multiple heterogeneous distributions could improve ceiling performance by mitigating distribution shift. If we accept this hypothesis, then it suggests that one may adopt a multiset training approach to identify limitations in a dataset. If we reject this hypothesis, then we are faced with two possibilities. The first possibility is that multiset training exhibits near ceiling performance, suggesting that the dataset has been optimally sampled and the inclusion of a broad training distribution does not aid generalization to new subjects. The second possibility is that multiset training exhibits deteriorated performance, suggesting that the network has limited complexity.

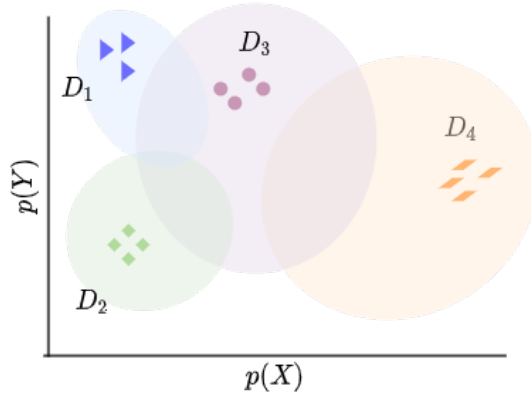


Fig. 1. An illustration to visualize two different training strategies one may adopt to maximize generalization. If D_3 represents a test distribution, then it is intuitive to train a model using a combination of D_1 , D_2 and D_4 . However, if D_4 represents a test distribution then a model specific to D_3 would demonstrate optimal generalization.

- In addition to the central hypothesis related to the principles of model generalization, we present multiple contributions and insights of practical use to the eye tracking community. These include analyzing the effects of data augmentation and model complexity.

2 RELATED WORK

Issues related to domain generalization arise when a ML model trained on a particular domain generally does not perform well on out-of-domain samples [30, 33, 44, 54, 59]. This well known phenomenon is known as distribution shift and generally occurs when the distribution of data points used to train the network does not match the distribution of data we are evaluating the model on. There are two major types forms of distributions shifts, prior and covariate shifts.

Prior shift occurs when the distribution of output labels between the train and test domains vary [33, 34]. Consider the case of eye image segmentation, a critical process in head-mounted eyetracking. In this context, a class could represent an annotated eye part at the pixel level (e.g. pupil, iris, sclera, other). A change in class proportions could occur when the eye camera is displaced to different distances or orientations not considered during training. To measure and mitigate prior shift, we require access to a small portion of labels from the test domain. Access to test labels allows us to selectively draw samples during training which better represent the test domain. Domain generalization however assumes no access to test labels. Data augmentation schemes such as artificially translating, rotating and scaling images from a domain can mitigate a portion of prior shift [43, 50, 52, 58, 61].

A mismatch in eye camera pose or gaze distributions is further convoluted by variation in eye image appearance. Appearances can widely vary depending on the environment, occlusions, subject physiology, pupil dilation, optical aberrations or reflections. Therefore, statistics related to the spatial distribution of group membership at the pixel level is unlikely to match across training/testing domains that reflect a difference in eye camera quality, camera intrinsic parameters, or across different populations and environments. Such a shift in distribution due to discordant appearances results in covariate shift. For example, a model trained to segment eye images captured indoors may not generalize well onto outdoor environments despite enforcing other variables such as a subject physiology, gaze position and camera pose to be fixed. There are numerous approaches

which attempt to minimize covariate shift but they require access to target imagery. Domain generalization assumes no access to target imagery.

2.1 Mitigating distribution shift

Previous work in domain generalization follow the intuition that a model may generalize better if internal network activations are invariant across domain-specific factors [16, 30, 54]. In the context of eyetracking, we want to encourage a network to learn a generalized representation of an eye image and its subsequent mapping to semantic categories which are invariant to camera quality, occluding artifacts, gaze position and eye camera location. This is achieved by penalizing a network when the learned latent representation of eye images statistically align themselves to the domain they were sampled from. Numerous attempts have been made which attempt to align representations across domains. Approaches involve leveraging the Mean Discrepancy metric [3, 37, 56], curriculum based learning [21], meta-learning [1, 9, 35] and adversarial learning [37, 49, 55] using min-max optimization [18] or gradient reversal [14].

While these techniques have demonstrated better generalization performance in their respective applications, their effectiveness for head-mounted eye image segmentation remains unclear. Extensive experiments by Gulrajani *et al.* [19] reveal that one of the earliest and simplest approaches, Empirical Risk Minimization (ERM) [59] results in similar or better performance as compared to state of the art approaches when implemented and evaluated correctly. Simply stated, ERM involves optimizing a model to minimize its risk of misclassification simultaneously across multiple domains. In this work, we refer to ERM as multiset training. Due to its simple and intuitive design, multiset training often serves as a baseline to measure other techniques for domain generalization. This work adopts multiset training to explore two hypotheses briefly introduced in the previous section by leveraging insights from Gulrajani *et al.*

3 METHODS

We describe the datasets, encoder-decoder convolutional architecture and various tests which allow us to test our hypothesis that jointly optimizing using multiple datasets results in better generalization than finding an optimal dataset to train a model.

3.1 Datasets

Tests of generalizability are complicated by practical limitations in dataset acquisition. Acquiring data which represents the general populace requires large-scale data collection with annotated ground truth. This needs many hours of tedious work, careful labelling, and may be impractical without the investment of significant time, financial resources, and coordinated effort across multiple laboratories. To mitigate this limitation, this work exploits multiple pre-existing and publicly available datasets of near-eye images acquired from a large number of subjects and different eye trackers which are captured under varying environmental conditions.

We acquire eye imagery from nine publicly available, annotated and heterogeneous datasets (see Table 1 for overall statistics, Supplementary Table 1 for dataset splitting procedure and Supplementary Figure 2 for individual distribution plots). Eye images from each dataset are assigned to a *train* or *test* split. Each split contains images acquired from different subjects or recording IDs. Images present in each dataset are scaled to a common resolution of 320×240 pixels. OpenEDS eye images were cropped vertically to maintain a constant aspect ratio across all datasets. Cropping was performed in a manner which ensured that the entire iris ellipse is visible. Note that the sets published in ExCuSe [10], ElSe [13] and PupilNet [12] are combined into a single dataset as the source of eye imagery are from the same collection [27]. We refer to the combination of these datasets as the *Fuhl* datasets.

Cond	Res	Status	Dataset	Subject ID		# of Images (Subjects)	
				Train	Test	Train	Test
Constrained	640×480	Synth	S-General	1 - 18	19 - 24	34254 (18)	11582 (6)
	400×640	Real	OpenEDS'19	Train set	Valid set	8827 (95)	2386 (28)
	1280×960	Synth	NVGaze	Male 1-4, Female 1-4	Male 5, Female 5	16000 (8)	4000 (2)
	640×480	Real	LPW*	2,4,5,7,10, 11,13,14,17, 19,21,22	3,6,8,9,12, 15,16,18,20	24000 (12)	17730 (10)
	640×480	Real	Swirski	1	2	298 (1)	298 (1)
	384×288	Real	BAT	1,2,3	4,5,6	3662 (3)	3541 (3)
Outdoors	640×480	Synth	S-Natural	1 - 18	19 - 24	34267 (18)	11548 (6)
	640×480	Synth	UnityEyes	-	-	16000 (-)	2000 (-)
	384×288	Real	(Fuhl) ExCuSe + ElSe + PupilNet	I, III, V, VII, VIII, XI, XII, XIV, XVI, XVIII, XIX, XX, XXI, XXIV, New II, New IV	II, IV, VI, IX, X, XIII, XV, XVII, XXII, XXIII, New I, New III, New V	73053 (16)	57496 (13)

Table 1. Datasets and their respective train and test splits used to explore generalization. Each dataset is classified into two broad categories called *outdoors* and *constrained*. Eye images in outdoor datasets exhibit large proportion of environmental reflections. Constrained datasets are acquired from experiments or synthetically rendered within indoor, lab environments with little to no reflective artifacts. * Approximately a third of LPW recordings were collected outdoors. Please see Supplementary Table 1 for details about the splitting process.

3.2 Network architecture

Drift-free [47] and parallax-free [17] eyetracking requires modelling the approximate 3D center of rotation of an eyeball from 2D pupil [5, 6, 28] or limbus ellipses [62]. This is achieved by segmenting an eye image into relevant categories and fitting ellipses to the pupil, iris and sclera boundaries. Convolutional encoder-decoder architectures have successfully been deployed to segment an eye image and extract pupil and iris ellipses [4, 11, 15, 32, 60, 64] for datasets with pixel-level semantic annotations. Most publicly available datasets do not provide access to pixel-level ground truth

annotation but instead provide the pupil center only. To circumvent this limitation, we adopt with minimal changes the EllSeg framework [32] that uniquely allows us to train a network using datasets with partial annotations. This is primarily achieved by tasking a convolutional network to segment entire elliptical masks instead of visible eye parts. The center of mass of the predicted elliptical maps allows us to optimize the entire architecture using only pupil and/or iris center annotations, conveniently allowing us to train a network on eye images with partial annotations [32]. For a complete breakdown of the architecture, please see Supplementary Figure 1.

3.3 Normalization scheme

Normalizing the input to a convolutional layer significantly speeds up training, improves peak accuracy performance, and reduces the dependence on weight initialization and hyper-parameter searches [22, 48]. Batch normalization in particular is a widely accepted technique to reparameterize the underlying optimization problem by providing a smoother loss landscape [48]. It computes μ_k and σ_k within a population sample (e.g. a *batch*) and approximates the global statistic by accumulating these values as training progresses. Statistics accumulated during the training phase are fixed during model evaluation and are generally provided alongside network parameters to facilitate inference.

Batch normalization is effective if statistics of the population sample accumulated during training are approximately equal to the global statistics of features extracted from the test set. This assumption is often violated in the context of domain generalization as statistics of the images we are evaluating our network on can be significantly different as compared to statistics observed during training. To overcome this limitation, we adopt Instance Normalization [57] as a drop-in replacement for Batch Normalization and observe improvements to generalization (see Supplementary Tables 5, 6 and 7). Instance Normalization computes the mean and standard deviation on a per image basis which are used to normalize and cast image features, irrespective of their domain, to the same unit-normal distribution.

3.4 Generalization tests

The primary goal of this work is to determine if training a model using multiple datasets results in better performance when generalized to an unseen domain as opposed to selecting the best performing domain-specific model. The former follows our intuitive understanding that training a model on multiple domains expands the available distribution we draw samples from. The latter is possible when the domain we are evaluating overlaps with an existing dataset. The adopted approach draws inspiration from Koshla *et al.* [30] and proposes four tests which allow us to explore our hypotheses. Every test below will be run on each individual domain's test set.

3.4.1 Within-dataset. This test is intended to measure the ceiling performance of a model for a given dataset's test set. Evaluating a model on the same dataset it was optimized on returns the upper performance limit. Any performance exceeding this measure indicates that a distribution gap exists between the train and test samples. This could occur if the dataset is limited by insufficient variability due to a biased sampling of its data distribution, insufficient number of subjects or limited gaze positions due to constrained tasks.

3.4.2 Cross-dataset. This test is intended to measure the performance of a model under conditions of cross-dataset Domain Generalization using a single training dataset. Cross dataset results indicate the performance of models when evaluated on domains not utilized during training. This test allows us to quantify how dissimilar two domains are based on their cross dataset performance measures. For every available dataset, this test allows us to empirically find the closest matching dataset.

3.4.3 All-vs-one. This test is intended to measure the ceiling level of performance when training utilizes all available datasets, including the within-domain dataset. This scheme trains a model using combined imagery from all available datasets. Comparing the performance of a model trained on all available distributions against its equivalent within-dataset performance gives us a clue about a single model's ability to capture information from multiple heterogeneous distributions. Deteriorated performance indicates insufficient network capacity and serves as a test to ensure that our results are not influenced by network architecture.

3.4.4 Leave-one-out. This test is intended to measure the performance of a model trained using multiple datasets except on a given test set that is used to evaluate the model performance. For example, leave-one-out results on the OpenEDS test set would involve training a model with all datasets except the OpenEDS training images. Comparing leave-one-out test results with cross-dataset performance provides evidence for the optimal strategy which maximally generalizes on the OpenEDS dataset.

3.5 Predictions

In this section, we briefly summarize expected results using the four proposed tests. Model performance will be reported on their relative ability to estimate the pupil and iris centers in units of pixels and mean Intersection-over-Union (mIoU) scores [7, 23, 51]. Systematic comparison across the proposed tests allows us to generate specific predictions directly related to our hypotheses.

3.5.1 Hypothesis 1: Cross-domain generalization. A single model trained on data drawn from multiple heterogeneous domains (the leave-one-out test) can generalize better than a specialized, dataset-specific model when evaluated on domains **unseen during training** (the cross-dataset test). This is achieved by comparing the leave-one-out test with the cross-dataset test. If the leave-one-out test leads to better generalization than the cross-dataset test, this would indicate that adding more datasets and acquiring a broader distribution will improve generalization, presumably asymptotically until the within-dataset performance limit is reached. If the cross-dataset model outperforms the leave-one-out test then it suggests that the best approach to achieve generalizability is to explore test-time techniques to find an optimal model from a pool of dataset-specific models, rather than to rely upon a single broadly-trained and general-purpose model.

3.5.2 Hypothesis 2: Within-domain generalization. Researchers often develop models for their specific applications with a fixed hardware setup and environmental conditions. This involves the collection and annotation of data we want to evaluate the model on. This is a time consuming, expensive process and researchers often collect and annotate a smaller subset with the aim of producing a model which generalizes to the entire breadth of data. However, a model may not generalize across subjects or gaze positions due to distribution shifts caused by limited or biased sampling of their specific distribution. The within-dataset performance represents the distribution shift exhibited when the train and test splits are sampled from the same distribution. We hypothesize that any remaining distribution shift due to biased sampling will be mitigated by increasing the breadth of training distribution. If this is true, then the all-vs-one test will outperform the within-dataset test. If the within-dataset test outperforms the all-vs-one test then it suggests that the all-vs-one model has insufficient complexity (parameters) to capture the entire breadth of the training data. Lastly, we can conclude that a dataset has been optimally sampled if both both tests exhibit nearly the same performance. All possibilities are explored in post-hoc tests and addressed in the discussion section.

3.5.3 Hypothesis 3: Effects of data augmentation. Data augmentation has numerous benefits for machine learning applications [20, 41]. It improves generalization by combating overfitting, expands

the training distribution and reduces domain gap by combating prior shifts. Previous work has demonstrated that domain-specific data augmentation significantly improves cross-subject performance in context of head-mounted eyetracking [8, 42]. Data augmentation is generally accepted as standard practice within Machine Learning and we quantify its effects on generalization.

It is plausible that within the context of eye image segmentation, data augmentation sufficiently reduces distribution shift by expanding the available training distribution while removing the need for multiset training. If this is true, then we expect cross-dataset tests to outperform the leave-one-out test. If this is false, then the inclusion of data augmentation is expected to improve performance across all tests while not affecting relative performance. Table 2 summarizes all augmentation schemes explored in this manuscript.

3.6 Analysis

Exploring our hypotheses for each dataset requires us to compare model performance between the proposed tests while keeping the within-dataset performance as baseline. However, datasets differ in complexity. A 1 pixel error improvement in pupil center estimation on a particular dataset cannot be compared objectively with others without considering the variability inherent within the ground truth, for the reason that one would expect more variability in model estimates for an inherently more variable test dataset. To mitigate this limitation, we consider the dispersion of test results (reported in median absolute deviation units, or MADs, due to its robustness to outliers) which are derived by normalizing a performance metric by the within-dataset test result.

3.7 Training details

This work relies on a modified version of DenseElNet [32], a standard encoder-decoder convolutional neural network inspired by RITNet [4], FC-DenseNet [24] and UNet [46]. Eye images are passed to the encoder which consists of 4 densely connected convolutional blocks. Each block extracts features from eye images while down-sampling their spatial extent by a factor of 2. Latent representations rich with semantic features are then fed into the decoder which produces a segmentation output mask for each eye image. For a complete breakdown of architecture, please refer to Supplementary Figure 1. Latent representations are also fed into a regression module which regresses pupil and iris ellipse parameters, if available.

For experiments which involve joint optimization on multiple datasets, an equal number of randomly selected samples from each domain are concatenated as input to our neural network. This process alleviates the concern of unequal representation due to a disproportionate number of samples in each domain (see Table 1). The validation set comprises 20% samples held out from the training set, either from a single or multiple domains. All models are optimized with ADAM [31] for 80 epochs. This work utilizes the loss functions proposed in EllSeg (Section 3.3 in Kothari *et al.* [32]). To curb overfitting and to ensure our model can be applied to both, left and right eyes, each eye image and its associated annotations are randomly flipped horizontally.

Experiments involving data augmentation modify input eye images and its associated annotations by randomly selecting an operation from a pool of augmentation schemes. Table 2 provides a summary of all schemes explored in this manuscript. Along with the ten data augmentation schemes introduced in Table 2, we also incorporate the possibility of not altering an eye image. Hence for any given eye image sample, we select one out of eleven possible choices, *i.e.*, each augmentation scheme has a $1/11$ chance of being selected.

3.8 Evaluation criterion

The performance of a model on a dataset is evaluated on a set of eye images (test set) from human subjects that were never present during training (see Table 1). Twenty percent of training

Gauss blur	Motion blur	Gamma	Exposure	Gauss noise
$w=7$ $\sigma=\mathcal{U}(2,7)$	$w=7$ $\theta=\mathcal{U}(0, \pi)$	$\gamma=\mathcal{U}(0.6, 1.4)$	$\Delta L_{max}^i = 0.8 \times \tilde{L}^i$ $\Delta L_{min}^i = 0.8 \times (255 - \tilde{L}^i)$ $L = L + \mathcal{U}(-\Delta L_{min}^i, \Delta L_{max}^i)$	$\mu=0$ $\sigma=\mathcal{U}(2, 16)$
Synth lines	Scale	Rotation	Translation	Synth fog
$\mathcal{U}(1,10)$ random white lines	Scale factor $\mathcal{U}(0.5, 0.9)$	$\theta=\mathcal{U}(-\pi, \pi)/4$	Horz: $\mathcal{U}(-W, W)/3$ Vert: $\mathcal{U}(-H, H)/3$	Please refer to <i>imgaug</i> [25]

Table 2. Augmentation schemes applied to every single eye image with a $1/11$ probability. The probability of $1/11$ reflects that there are 10 possible augmentations in addition to the lack of augmentation. \mathcal{N} and \mathcal{U} indicate a normal and uniform distribution respectively. The median iris intensity \hat{L} , if available, or a range of ± 50 intensity levels is utilized during image exposure augmentation.

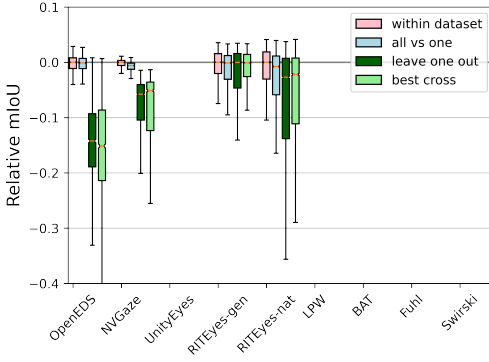
data is withheld for model validation during training. The best performing model is selected as the configuration which maximizes an average of mIoU and $d_i + d_p$ on the validation set. Here, $d_p = 1 - \alpha e_p$ and $d_i = 1 - \alpha e_i$ where e_p and e_i are pixel errors in predicting the pupil and iris centers and $\alpha = 1/240$ is derived from the smallest image dimension. All models are evaluated every 2000 *iterations*, wherein an iteration is defined as a single network parameter update operation based on a batch of eye images. Annotations not present in a dataset are ignored while computing the evaluation metric. For experiments which involve training on multiple datasets, each batch consists of 3 eye images extracted randomly from every dataset included in the experiment. For experiments involving training on a single dataset, each batch consists of 24 eye images.

3.9 Hypothesis 1: Training with multiple datasets is an optimal strategy for generalization.

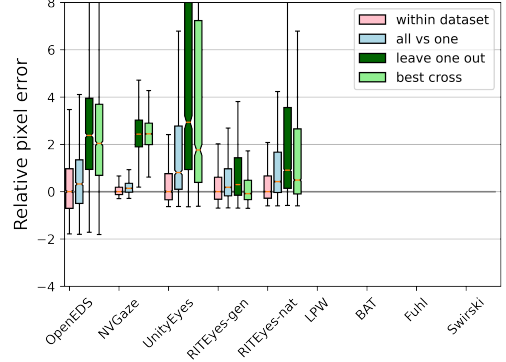
4 RESULTS AND DISCUSSION

In this section, we provide results for tests listed in Section 3.4. We focus our observations primarily on datasets with real eye images since observations on synthetic datasets do not support evidence for generalization during naturalistic conditions. We report our results on three separate metrics of performance. The pupil and iris center error which is measured in pixel units, and the mIoU score measured as the fraction of intersection to the union of the predicted and groundtruth categories of each pixel. Note that only the ground truth pupil center annotations are available for the majority of datasets with real eye imagery with the exception of OpenEDS, which contains all annotations. Hence, our analysis primarily focuses on pupil center performance with specific observations made for datasets with annotated iris centers and segmentation masks.

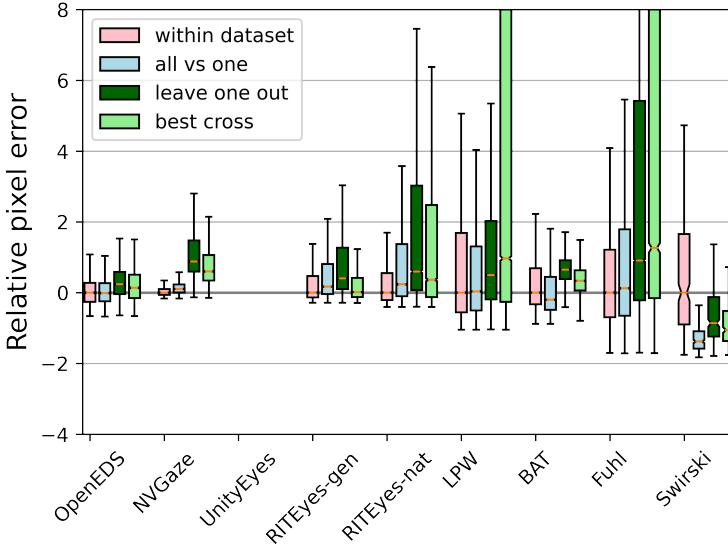
Figure 2 reveals that a multiset model offers improvements to generalization as opposed to selecting any dataset specific model for the LPW and Fuhl datasets (LPW $\uparrow 0.66$ MADs, Fuhl $\uparrow 0.42$ MADs). This is evident when comparing the best performing cross-dataset test result with the leave-one-out test. However, results indicate the opposite to be true for OpenEDS, BAT and Swirski datasets ($\downarrow 0.37$, $\downarrow 0.71$ and $\downarrow 0.18$ respectively). One explanation for this behavior is the conditions which these dataset represent. The Fuhl datasets were collected from subjects tasked to drive a car outdoors while subjects in LPW were tasked to fixate on a red ball moved by an experimenter in a variety of environmental conditions. In contrast, OpenEDS, BAT and Swirski datasets consist of physically restrained subjects who were given tasks which elicited a narrow range of gaze positions.



(a) Performance measured as the mIoU metric. The Y axis represents IoU score relative to the control condition, *within-dataset*. Positive values indicate a performance improvement.



(b) Error in iris center, e_i , in pixels. The Y axis represents pixel distance relative to the control condition, *within-dataset*. Negative values indicate a performance improvement.



(c) Error in pupil center, e_p , in pixels. The Y axis represents pixel distance relative to the control condition, *within-dataset*. Negative values indicate a performance improvement.

Fig. 2. Generalization test results. Each box plot highlights a model's performance centered to the within-dataset limit for each domain. The line and notch present within each box plot represents the median and 95% confidence interval respectively while the ends of each box denotes the 1st and 3rd quartile. All images are 320×240 resolution. Note that datasets which are missing groundtruth annotations do not have a boxplot entry. All measures are reported relative to the within-dataset performance, which necessarily lies at zero. The absolute performance of various tests are provided in Supplementary Tables 2, 3 and 4

Furthermore, eye images in these datasets were collected under constrained conditions with fixed lighting. This observation alludes to the variability of eye images inherent in these datasets.

To further analyze the dimensions along which these datasets vary, we performed a post-hoc analysis on the pupil location and appearance across eye images in every dataset present (see Supplementary Figure 2). We observe that eye images in the LPW and Fuhl datasets exhibit a broader distribution of pupil positions. They also demonstrate higher variability in the proportion of iris pixels across eye images. Humans exhibit relatively constant iris size when compared to the pupil, which frequently constricts and dilates. A large variation in proportion of iris pixels indicates a wider range of eye camera orientation and position. This is verified by Tonsen *et al.* who frequently varied the eye camera pose between frontal to off-axis views to capture a broader appearance of eye images [53]. Furthermore, the luminance distribution of pupils in these two datasets demonstrate a large spread and significant presence of intensities above the mean luminance of an eye image. Note that due to the absence of groundtruth, the luminance distribution of pupil regions is derived from predicted segmentation masks in Supplementary Figure 2.

The multiset training paradigm also demonstrates an improvement in segmentation performance on the OpenEDS ($\uparrow 0.95$ MADs). This evidence supports the intuition that multiset training offers a broader range of iris appearances which in turn has the potential to improve iris segmentation. To summarize, our analysis supports the conclusion that a multiset training paradigm offers better generalization as opposed to selecting the best performing cross-dataset model for eye images acquired under conditions with high variability.

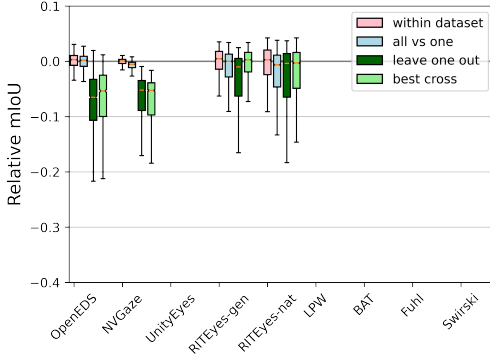
4.1 Hypothesis 2: Training with multiple datasets will improve within-dataset performance.

The within-dataset performance represents the distribution shift exhibited when the train and test splits are sampled from the same distribution. We hypothesize that training with multiple heterogeneous distributions could improve upon the within-dataset performance by mitigating this latent distribution shift. That is to say we hypothesize that in the presence of distribution shift, the shift will be mitigated by increasing the breadth of the training distribution, as would be suggested if the all-vs-one test were to outperform the within dataset test. However, results indicate that it is only on the BAT and Swirski datasets that the all-vs-one test outperforms the within-dataset performance, by 0.45 and 1.34 MADs, respectively. For the majority of the datasets, the all-vs-one model demonstrates only a slight reduction in performance from the expected within-dataset upper bound. The highest disagreement with the upper bound is evidenced on the Fuhl dataset with $\downarrow 0.146$, on the pupil center upper bound respectively.

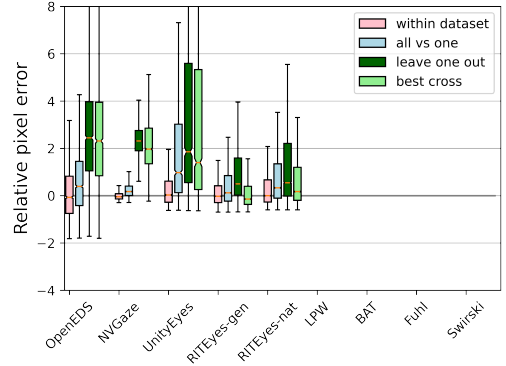
Closer inspection reveals that the Swirski dataset is comprised of ~ 300 eye images from a single subject and that the BAT dataset consists of 3.5K eye images from 3 subjects. This is evidenced by the sparse pupil center distribution and the poor overlap exhibited by the train and test eye images (see Supplemental Figure 2). Results indicate that these datasets are insufficient for cross-subject generalization despite their images being drawn from the same environment and eyetracker hardware. This limitation is mitigated by the all-vs-one model which provides a broad training distribution and improving generalization to new subjects.

4.2 Hypothesis 3: Effects of data augmentation for generalization

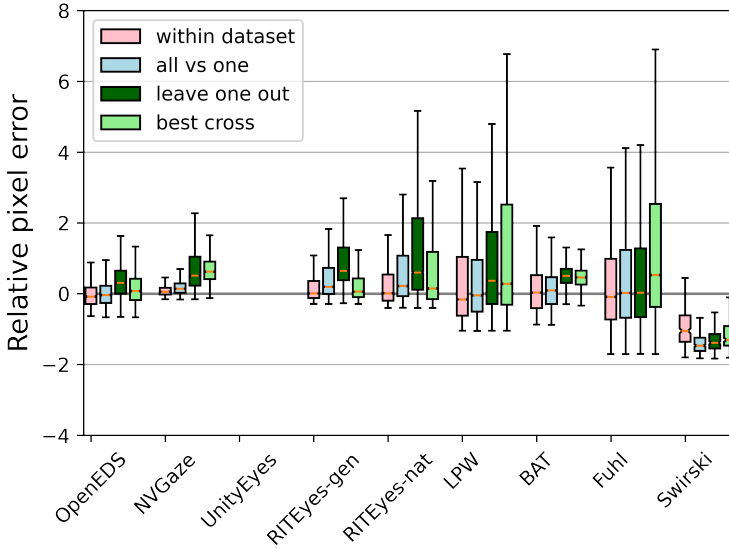
Figure 3 summarizes performance gains observed by augmenting eye images, and reveals that data augmentation improves performance across all testing sets. This is indicated by reductions in the inter-quartile range and improvements to the median performance across all metrics and tests.



(a) Performance following data augmentation measured as the mIoU metric relative to training in the absence of augmentation. Positive values indicate an improvement in performance.



(b) Performance following data augmentation measured as error in iris center, e_i , in pixels. Negative values indicate an improvement in performance.



(c) Performance following data augmentation measured as error in pupil center e_p in pixels. Negative values indicate an improvement in performance.

Fig. 3. Generalization test results to study the effects of data augmentation. Each box plot highlights a model's performance centered to the within-dataset limit for each domain. The line and notch present within each box plot represents the median and confidence interval respectively while the ends of each box denotes the 1st and 3rd quartile. All images are 320×240 resolution. Note that boxplots pertaining to datasets without a certain groundtruth annotation are missing. All measures are centered to the within-dataset threshold without data augmentation as reported in Figure 2 and Supplementary Tables 2, 3 and 4

We find that our previous established hypotheses (see Section 4.1) regarding multiset training remains unaffected by the presence of data augmentation. Significant improvements to generalization can be observed on the Fuhl datasets wherein a combination of multiset training and data augmentation achieves performance on par with the within-dataset baseline.

Our tests of hypothesis 1 revealed that the LPW dataset favors multiset training, possibly due to its relatively wide distribution of pupil center locations. As expected, data augmentation sufficiently reduces the performance gap between the multiset model and the best performing cross-dataset model (albeit with a higher spread), indicating that either approach for generalization returns similar performance. Please see Figure 4 to visualize the performance of a multiset model in leave-one-out configuration.

In hypothesis 2, we identified that multiset training aids in overcoming the effects of limited sampling. Previously, the BAT all-vs-one test outperformed the within-dataset baseline indicating a distribution shift between its own train and test set. This shift is entirely eliminated by artificially augmenting eye images. The multiset training however outperforms the within-dataset baseline for the Swirski dataset, indicating that data augmentation alone does not sufficiently expand the training distribution for datasets with significant limited sampling.

4.3 Effects of reducing model complexity

Head-mounted eyetracking is primarily used for studying eye movements during unconstrained activities. This requires algorithms or models to be computationally inexpensive in order to conserve battery or reduce system latency to support downstream applications which rely on gaze estimates. The model employed in this work contains 2.24 million trainable parameters and operates at 118Hz on a NVIDIA RTX3090. When the number of trainable parameters was reduced to 529K, performance speed increased to 140Hz. Although this increase in speed is accompanied by an overall reduction in model performance across all tests, the ordinal relationships between tests remain unaffected by model complexity (see Supplementary Figure 3).

5 CONCLUSION

In this work, we have explored the task of Domain Generalization for segmenting near infrared eye images. This was achieved by jointly optimizing an encoder-decoder network on multiple eye image datasets with the intuition that a model would learn a generalized representation of eye images and elliptical eye parts. This work evaluated two approaches towards generalization, a) a multiset training approach to produce a single, robust model or b) pick the best performing model from a pool of pretrained, dataset-specific models. Generalization results indicate that datasets which exhibit higher variability benefit from multiset optimization. In contrast, dataset-specific models generalize better onto constrained use-cases, such as eye tracking applications where the eye camera properties are fixed, camera pose is constrained, and lighting conditions are controlled.

Although a model's peak performance can be attained when it is trained and evaluated on data sampled from the same source distribution, limited or biased sampling often leads to a distribution shift and deteriorated model performance. Results indicate that multiset training can be utilized to identify and mitigate such a distribution shift, if it exists. This work also validates the benefits of data augmentation to further improve generalization by observing improvements in model performance across the board. Results indicate that a combination of data augmentation and multiset training attains the peak performance recorded for unconstrained eye images. While data augmentation does improve performance, it does not invalidate the contributions of multiset learning but instead,

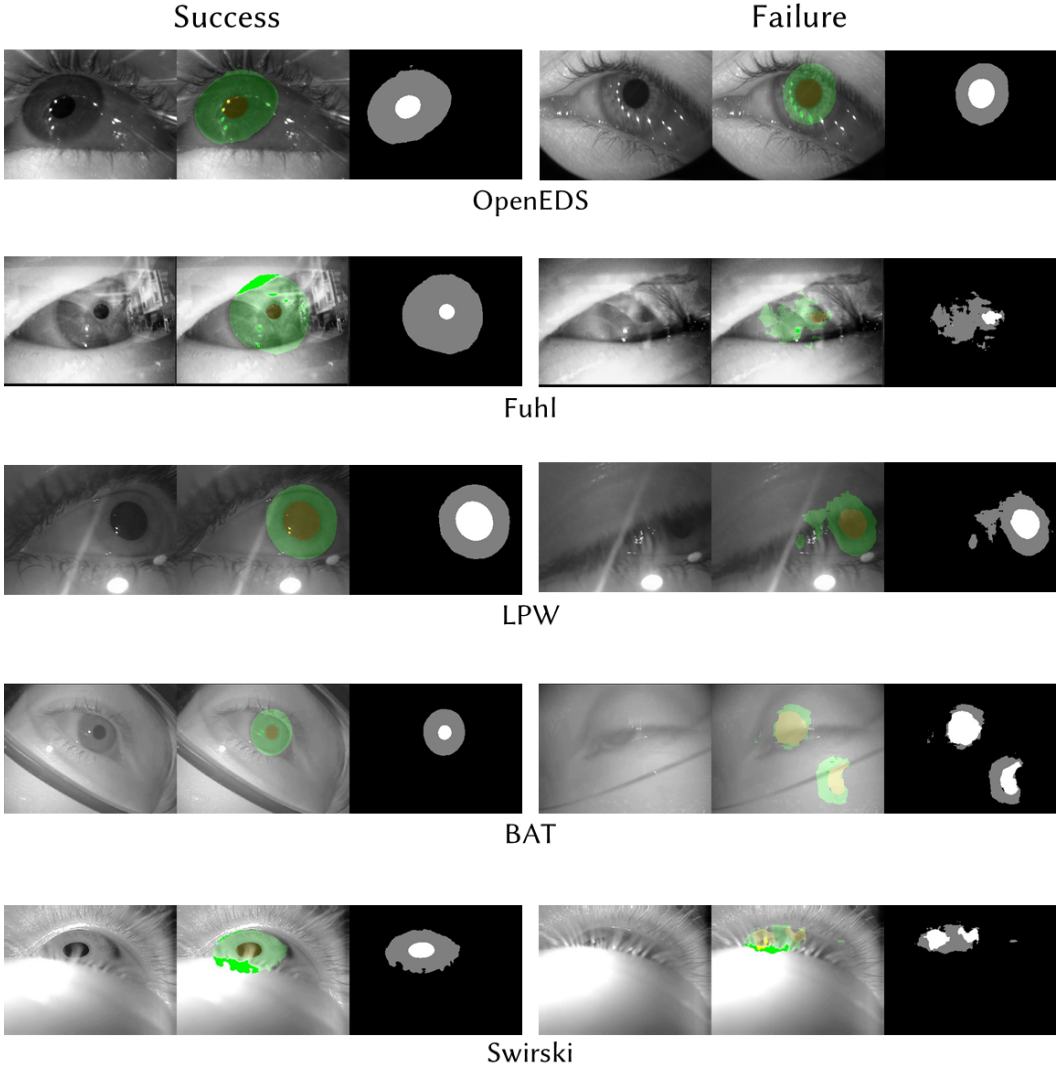


Fig. 4. Success and failure examples of DenseINet predictions in the leave-one-out configuration. Note that for any eye image shown in this figure, not a single image from its domain/dataset was used to train the model. This figure is representative of what to expect during model deployment on the datasets shown.

complements it. Models and code to facilitate our experiments are publicly available¹ for the research community.

ACKNOWLEDGMENTS

The authors thank Research Computing at the Rochester Institute of Technology for their support and providing necessary hardware. The authors would also like to thank Dr. Aneesh Rangnekar for their helpful comments and feedback.

¹bitbucket.org/RSKothari/multiset_gaze/src

REFERENCES

- [1] Yogesh Balaji, Swami Sankaranarayanan, and Rama Chellappa. 2018. Metareg: Towards domain generalization using meta-regularization. *Advances in Neural Information Processing Systems* 2018-Decem, NeurIPS (2018), 998–1008.
- [2] Shai Ben-David, John Blitzer, Koby Crammer, Alex Kulesza, Fernando Pereira, and Jennifer Wortman Vaughan. 2010. A theory of learning from different domains. *Machine learning* 79, 1-2 (2010), 151–175.
- [3] Karsten M Borgwardt, Arthur Gretton, Malte J Rasch, Hans-Peter Kriegel, Bernhard Schölkopf, and Alex J Smola. 2006. Integrating structured biological data by kernel maximum mean discrepancy. *Bioinformatics* 22, 14 (2006), e49–e57.
- [4] Aayush K. Chaudhary, Rakshit Kothari, Manoj Acharya, Shusil Dangi, Nitinraj Nair, Reynold Bailey, Christopher Kanan, Gabriel Diaz, and Jeff B. Pelz. 2019. RiTnet: Real-time semantic segmentation of the eye for gaze tracking. In *Proceedings - 2019 International Conference on Computer Vision Workshop, ICCVW 2019*. IEEE, 3698–3702. <https://doi.org/10.1109/ICCVW.2019.00568> arXiv:1910.00694
- [5] Kai Dierkes, Moritz Kassner, and Andreas Bulling. 2018. A novel approach to single camera, glint-free 3D eye model fitting including corneal refraction. *Eye Tracking Research and Applications Symposium (ETRA)* June (2018). <https://doi.org/10.1145/3204493.3204525>
- [6] Kai Dierkes, Moritz Kassner, and Andreas Bulling. 2019. A fast approach to refraction-aware eye-model fitting and gaze prediction. June (2019), 1–9. <https://doi.org/10.1145/3314111.3319819>
- [7] Tom Eelbode, Jeroen Bertels, Maxim Berman, Dirk Vandermeulen, Frederik Maes, Raf Bisschops, and Matthew B Blaschko. 2020. Optimization for medical image segmentation: theory and practice when evaluating with Dice score or Jaccard index. *IEEE Transactions on Medical Imaging* 39, 11 (2020), 3679–3690.
- [8] Shaharam Eivazi, Thiago Santini, Alireza Keshavarzi, Thomas Kübler, and Andrea Mazzei. 2019. Improving real-time CNN-based pupil detection through domain-specific data augmentation. (2019), 1–6. <https://doi.org/10.1145/3314111.3319914>
- [9] Chelsea Finn, Pieter Abbeel, and Sergey Levine. 2017. Model-agnostic meta-learning for fast adaptation of deep networks. In *International Conference on Machine Learning*. PMLR, 1126–1135.
- [10] Wolfgang Fuhl, Thomas Kübler, Katrin Sippel, Wolfgang Rosenstiel, and Enkelejda Kasneci. 2015. Excuse: Robust pupil detection in real-world scenarios. In *International conference on computer analysis of images and patterns*. Springer, 39–51.
- [11] Wolfgang Fuhl, Wolfgang Rosenstiel, and Enkelejda Kasneci. 2019. *500,000 Images Closer to Eyelid and Pupil Segmentation*. Lecture Notes in Computer Science, Vol. 11678 LNCS. Springer International Publishing, Cham. 336–347 pages. https://doi.org/10.1007/978-3-030-29888-3_27
- [12] Wolfgang Fuhl, Thiago Santini, Gjergji Kasneci, Wolfgang Rosenstiel, and Enkelejda Kasneci. 2017. PupilNet v2.0: Convolutional Neural Networks for CPU based real time Robust Pupil Detection. (2017). <http://arxiv.org/abs/1711.00112>
- [13] Wolfgang Fuhl, Thiago C. Santini, Thomas Kübler, and Enkelejda Kasneci. 2016. ElSe: Ellipse selection for robust pupil detection in real-world environments. In *Eye Tracking Research and Applications Symposium (ETRA)*, Vol. 14. 123–130. <https://doi.org/10.1145/2857491.2857505>
- [14] Yaroslav Ganin and Victor Lempitsky. 2015. Unsupervised domain adaptation by backpropagation. In *International conference on machine learning*. PMLR, 1180–1189.
- [15] Stephan J. Garbin, Yiru Shen, Immo Schuetz, Robert Cavin, Gregory Hughes, and Sachin S. Talathi. 2019. OpenEDS: Open Eye Dataset. (2019). <http://arxiv.org/abs/1905.03702>
- [16] Muhammad Ghifary, W Bastiaan Kleijn, Mengjie Zhang, and David Balduzzi. 2015. Domain generalization for object recognition with multi-task autoencoders. In *Proceedings of the IEEE international conference on computer vision*. 2551–2559.
- [17] Agostino Gibaldi, Vasha DuTell, and Martin S Banks. 2021. Solving Parallax Error for 3D Eye Tracking. In *ACM Symposium on Eye Tracking Research and Applications*. 1–4.
- [18] Ian Goodfellow, Jean Pouget-Abadie, Mehdi Mirza, Bing Xu, David Warde-Farley, Sherjil Ozair, Aaron Courville, and Yoshua Bengio. 2014. Generative adversarial nets. *Advances in neural information processing systems* 27 (2014).
- [19] Ishaan Gulrajani and David Lopez-Paz. 2020. In Search of Lost Domain Generalization. (2020). arXiv:2007.01434 <http://arxiv.org/abs/2007.01434>
- [20] Alex Hernández-García and Peter König. 2018. Further advantages of data augmentation on convolutional neural networks. In *International Conference on Artificial Neural Networks*. Springer, 95–103.
- [21] Bincheng Huang, Si Chen, Fan Zhou, Cheng Zhang, and Feng Zhang. 2020. Episodic Training for Domain Generalization Using Latent Domains. In *International Conference on Cognitive Systems and Signal Processing*. Springer, 85–93.
- [22] Sergey Ioffe and Christian Szegedy. 2015. Batch normalization: Accelerating deep network training by reducing internal covariate shift. In *International conference on machine learning*. PMLR, 448–456.
- [23] Paul Jaccard. 1912. The distribution of the flora in the alpine zone. 1. *New phytologist* 11, 2 (1912), 37–50.
- [24] Simon Jegou, Michal Drozdal, David Vazquez, Adriana Romero, and Yoshua Bengio. 2017. The One Hundred Layers Tiramisu: Fully Convolutional DenseNets for Semantic Segmentation. *IEEE Computer Society Conference on Computer*

- Vision and Pattern Recognition Workshops* 2017-July (2017), 1175–1183. <https://doi.org/10.1109/CVPRW.2017.156>
- [25] Alexander B. Jung, Kentaro Wada, Jon Crall, Satoshi Tanaka, Jake Graving, Christoph Reinders, Sarthak Yadav, Joy Banerjee, Gábor Vecsei, Adam Kraft, Zheng Rui, Jirka Borovec, Christian Vallentin, Semen Zhydenko, Kilian Pfeiffer, Ben Cook, Ismael Fernández, François-Michel De Rainville, Chi-Hung Weng, Abner Ayala-Acevedo, Raphael Meudec, Matias Laporte, et al. 2020. imgaug. <https://github.com/aleju/imgaug>. Online; accessed 01-Feb-2020.
- [26] Priya Kansal and Sabarinathan Devanathan. 2019. Eyenet: Attention based convolutional encoder-decoder network for eye region segmentation. In *2019 IEEE/CVF International Conference on Computer Vision Workshop (ICCVW)*. IEEE, 3688–3693.
- [27] Enkelejda Kasneci, Katrin Sippel, Kathrin Aehling, Martin Heister, Wolfgang Rosenstiel, Ulrich Schiefer, and Elena Papageorgiou. 2014. Driving with binocular visual field loss? A study on a supervised on-road parcours with simultaneous eye and head tracking. *PLoS one* 9, 2 (2014), e87470.
- [28] Moritz Kassner, William Patera, and Andreas Bulling. 2014. Pupil: An open source platform for pervasive eye tracking and mobile gaze-based interaction. *UbiComp 2014 - Adjunct Proceedings of the 2014 ACM International Joint Conference on Pervasive and Ubiquitous Computing* (2014), 1151–1160. <https://doi.org/10.1145/2638728.2641695>
- [29] Alex Kendall and Yarin Gal. 2017. What uncertainties do we need in bayesian deep learning for computer vision? *Advances in neural information processing systems* 30 (2017).
- [30] Aditya Khosla, Tinghui Zhou, Tomasz Malisiewicz, Alexei A. Efros, and Antonio Torralba. 2012. Undoing the damage of dataset bias. *Lecture Notes in Computer Science (including subseries Lecture Notes in Artificial Intelligence and Lecture Notes in Bioinformatics)* 7572 LNCS, PART 1 (2012), 158–171. https://doi.org/10.1007/978-3-642-33718-5_12
- [31] Diederik P. Kingma and Jimmy Ba. 2014. Adam: A Method for Stochastic Optimization. *AIP Conference Proceedings* 1631, 2 (12 2014), 58–62. <https://doi.org/10.1016/j.jneumeth.2005.04.009>
- [32] Rakshit S Kothari, Aayush K Chaudhary, Reynold J Bailey, Jeff B Pelz, and Gabriel J Diaz. 2021. EllSeg: An Ellipse Segmentation Framework for Robust Gaze Tracking. *IEEE Transactions on Visualization and Computer Graphics* 27, 5 (2021), 2757–2767.
- [33] Wouter M Kouw and Marco Loog. 2018. An introduction to domain adaptation and transfer learning. *arXiv preprint arXiv:1812.11806* (2018).
- [34] Wouter Marco Kouw and Marco Loog. 2019. A review of domain adaptation without target labels. *IEEE transactions on pattern analysis and machine intelligence* (2019).
- [35] Da Li, Yongxin Yang, Yi-Zhe Song, and Timothy Hospedales. 2018. Learning to generalize: Meta-learning for domain generalization. In *Proceedings of the AAAI Conference on Artificial Intelligence*, Vol. 32.
- [36] Da Li, Yongxin Yang, Yi-Zhe Song, and Timothy M Hospedales. 2017. Deeper, broader and artier domain generalization. In *Proceedings of the IEEE international conference on computer vision*. 5542–5550.
- [37] Haoliang Li, Sinno Jialin Pan, Shiqi Wang, and Alex C Kot. 2018. Domain generalization with adversarial feature learning. In *Proceedings of the IEEE Conference on Computer Vision and Pattern Recognition*. 5400–5409.
- [38] Aleksander Madry, Aleksandar Makelov, Ludwig Schmidt, Dimitris Tsipras, and Adrian Vladu. 2017. Towards deep learning models resistant to adversarial attacks. *arXiv preprint arXiv:1706.06083* (2017).
- [39] Krikamol Muandet, David Balduzzi, and Bernhard Schölkopf. 2013. Domain generalization via invariant feature representation. *30th International Conference on Machine Learning, ICML 2013 PART 1* (2013), 10–18. [arXiv:1301.2115](https://arxiv.org/abs/1301.2115)
- [40] Nitinraj Nair, Rakshit Kothari, Aayush K Chaudhary, Zhizhuo Yang, Gabriel J Diaz, Jeff B Pelz, and Reynold J Bailey. 2020. RIT-Eyes: Rendering of near-eye images for eye-tracking applications. In *ACM Symposium on Applied Perception* 2020. 1–9.
- [41] Jakub Nalepa, Michal Marcinkiewicz, and Michal Kawulok. 2019. Data augmentation for brain-tumor segmentation: a review. *Frontiers in computational neuroscience* 13 (2019), 83.
- [42] Seonwook Park, Adrian Spurr, and Otmar Hilliges. 2018. Deep Pictorial Gaze Estimation. Vol. 11217 LNCS. 741–757. https://doi.org/10.1007/978-3-030-01261-8_44
- [43] Seonwook Park, Xucong Zhang, Andreas Bulling, and Otmar Hilliges. 2018. Learning to find eye region landmarks for remote gaze estimation in unconstrained settings. In *Eye Tracking Research and Applications Symposium (ETRA)*. ACM Press, New York, New York, USA, 1–10. <https://doi.org/10.1145/3204493.3204545>
- [44] Jean Ponce, Tamara L Berg, Mark Everingham, David A Forsyth, Martial Hebert, Svetlana Lazebnik, Marcin Marszałek, Cordelia Schmid, Bryan C Russell, Antonio Torralba, et al. 2006. Dataset issues in object recognition. In *Toward category-level object recognition*. Springer, 29–48.
- [45] Aditi Raghunathan, Sang Michael Xie, Fanny Yang, John Duchi, and Percy Liang. 2020. Understanding and mitigating the tradeoff between robustness and accuracy. *arXiv preprint arXiv:2002.10716* (2020).
- [46] Olaf Ronneberger, Philipp Fischer, and Thomas Brox. 2015. U-net: Convolutional networks for biomedical image segmentation. 9351 (2015), 234–241. https://doi.org/10.1007/978-3-319-24574-4_28
- [47] Thiago Santini, Diederick C. Niehorster, and Enkelejda Kasneci. 2019. Get a grip: Slippage-robust and glint-free gaze estimation for real-time pervasive head-mounted eye tracking. *Eye Track. Res. Appl. Symp.* (2019). <https://doi.org/10.1145/3291111.3291112>

[//doi.org/10.1145/3314111.3319835](https://doi.org/10.1145/3314111.3319835)

- [48] Shibani Santurkar, Dimitris Tsipras, Andrew Ilyas, and Aleksander Madry. 2018. How does batch normalization help optimization?. In *Proceedings of the 32nd international conference on neural information processing systems*. 2488–2498.
- [49] Yiru Shen, Oleg Komogortsev, and Sachin S Talathi. 2020. Domain Adaptation for Eye Segmentation. In *European Conference on Computer Vision*. Springer, 555–569.
- [50] Connor Shorten and Taghi M Khoshgoftaar. 2019. A survey on image data augmentation for deep learning. *Journal of Big Data* 6, 1 (2019), 1–48.
- [51] TT Tanimoto. 1968. An elementary mathematical theory of classification and prediction, IBM Report (November, 1958), cited in: G. Salton, Automatic Information Organization and Retrieval.
- [52] Martin A Tanner and Wing Hung Wong. 1987. The calculation of posterior distributions by data augmentation. *Journal of the American statistical Association* 82, 398 (1987), 528–540.
- [53] Marc Tonsen, Xucong Zhang, Yusuke Sugano, and Andreas Bulling. 2016. Labelled pupils in the wild: a dataset for studying pupil detection in unconstrained environments. In *Proceedings of the ninth biennial ACM symposium on eye tracking research & applications*. 139–142.
- [54] Antonio Torralba and Alexei A Efros. 2011. Unbiased look at dataset bias. In *CVPR 2011*. IEEE, 1521–1528.
- [55] Eric Tzeng, Judy Hoffman, Kate Saenko, and Trevor Darrell. 2017. Adversarial discriminative domain adaptation. In *Proceedings of the IEEE conference on computer vision and pattern recognition*. 7167–7176.
- [56] Eric Tzeng, Judy Hoffman, Ning Zhang, Kate Saenko, and Trevor Darrell. 2014. Deep domain confusion: Maximizing for domain invariance. *arXiv preprint arXiv:1412.3474* (2014).
- [57] Dmitry Ulyanov, Andrea Vedaldi, and Victor Lempitsky. 2016. Instance normalization: The missing ingredient for fast stylization. *arXiv preprint arXiv:1607.08022* (2016).
- [58] David A Van Dyk and Xiao-Li Meng. 2001. The art of data augmentation. *Journal of Computational and Graphical Statistics* 10, 1 (2001), 1–50.
- [59] Vladimir N Vapnik. 1999. An overview of statistical learning theory. *IEEE transactions on neural networks* 10, 5 (1999), 988–999.
- [60] F. J. Vera-Olmos, E. Pardo, H. Melero, and N. Malpica. 2018. DeepEye: Deep convolutional network for pupil detection in real environments. *Integrated Computer-Aided Engineering* 26, 1 (2018), 85–95. <https://doi.org/10.3233/ICA-180584>
- [61] Jason Wang, Luis Perez, et al. 2017. The effectiveness of data augmentation in image classification using deep learning. *Convolutional Neural Networks Vis. Recognit* 11 (2017), 1–8.
- [62] Erroll Wood and Andreas Bulling. 2014. Eyetab: Model-based gaze estimation on unmodified tablet computers. In *Proceedings of the symposium on eye tracking research and applications*. 207–210.
- [63] Yao-Yuan Yang, Cyrus Rashtchian, Hongyang Zhang, Russ R Salakhutdinov, and Kamalika Chaudhuri. 2020. A closer look at accuracy vs. robustness. *Advances in neural information processing systems* 33 (2020), 8588–8601.
- [64] Yuk-Hoi Yiu, Moustafa Aboulatta, Theresa Raiser, Leoni Ophey, Virginia L. Flanagan, Peter zu Eulenburg, and Seyed-Ahmad Ahmadi. 2019. DeepVOG: Open-source pupil segmentation and gaze estimation in neuroscience using deep learning. *Journal of Neuroscience Methods* 324 (2019), 108307. <https://doi.org/10.1016/j.jneumeth.2019.05.016>
- [65] Hongyang Zhang, Yaodong Yu, Jiantao Jiao, Eric Xing, Laurent El Ghaoui, and Michael Jordan. 2019. Theoretically principled trade-off between robustness and accuracy. In *International Conference on Machine Learning*. PMLR, 7472–7482.

Received November 2021; revised January 2022; accepted April 2022

SUPPLEMENTARY DATA

Dataset	Splitting procedure	Test to train ratio of subjects	Test to train ratio of images
S-General	Maintain splits adopted in Nair	0.33	0.3
OpenEDS'19	Adopted splits proposed by Garbin	0.29	0.27
NVGaze	Random selection	0.25	0.25
LPW	Previously reported pupil detection rates by Fuhl was utilized to categorize each subset as <i>difficult</i> or <i>easy</i> . Each subset was assigned to the train and test split such that the number of <i>difficult</i> and <i>easy</i> subsets remained the same in both splits.	0.83	0.73
Swirski	We chose to place subject 2 in the test split due to the eye camera positioned in an off-axis configuration	1	
BAT	Subjects 1 and 4 wore glasses which was presumed to represent difficult conditions for our eye image segmentation model. We ensured difficult conditions were present in both train and test splits by assigning subject 1 to the train split and subject 4 to the test split.	1	0.96
S-Natural	Maintain splits adopted in Nair	0.33	0.33
UnityEyes	Random selection	-	0.12
Fuhl	Previously reported pupil detection rates by Fuhl was utilized to categorize each subset as a <i>difficult</i> or <i>easy</i> . Each subset was assigned to the train and test split such that the overall number of <i>difficult</i> and <i>easy</i> subsets remained the same.	0.81	0.78

Table 1. Splitting criterion employed while generating individual train and test splits for each dataset

Train on / Test on	OpenEDS	NVGaze	UnityEyes	RI TEyes-Gen	RI TEyes-Nat	LPW	BAT	Fuhl	Swirski
OpenEDS	0.957	0.670		0.576	0.419				
NVGaze	0.652	0.988		0.563	0.362				
UnityEyes									
RI TEyes-Gen	0.796	0.936		0.962	0.933				
RI TEyes-Nat	0.806	0.932		0.961	0.955				
LPW									
Santini									
Fuhl									
Swirski									
all-OpenEDS	0.815	0.985		0.977	0.965				
all-NVGaze	0.960	0.930		0.974	0.965				
all-UnityEyes	0.960	0.983		0.973	0.961				
all-RI TEyes-Gen	0.961	0.983		0.962	0.958				
all-RI TEyes-Nat	0.960	0.984		0.968	0.928				
all-LPW	0.960	0.984		0.974	0.962				
all-Santini	0.961	0.984		0.976	0.965				
all-Fuhl	0.961	0.984		0.975	0.964				
all-Swirski	0.960	0.985		0.977	0.968				
all	0.956	0.982		0.961	0.947				

Table 2. Segmentation results of various generalization tests proposed in Section 3.4. All results represent the IoU metric.

Train on / Test on	OpenEDS	NVGaze	UnityEyes	RI TEyes-Gen	RI TEyes-Nat	LPW	BAT	Fuhl	Swirski
OpenEDS	0.683	1.925		7.970	23.625	2.462	2.406	7.736	1.732
NVGaze	1.039	0.168		17.104	30.998	10.507	1.227	70.052	4.736
UnityEyes									
RI TEyes-Gen	0.845	0.850		0.292	0.768	2.019	1.540	12.642	0.987
RI TEyes-Nat	0.818	0.767		0.305	0.407	2.122	2.366	2.985	1.623
LPW	1.152	3.037		12.014	32.724	1.052	1.308	17.489	0.788
Santini	2.912	94.254		31.814	54.246	12.778	0.892	94.609	2.105
Fuhl	1.060	0.867		4.122	8.896	3.133	1.444	1.719	1.731
Swirski	4.272	169.359		35.463	71.910	13.786	2.911	98.026	1.844
all-OpenEDS	0.918	0.240		0.378	0.529	0.894	0.412	1.717	0.240
all-NVGaze	0.666	1.048		0.453	0.624	0.960	0.438	1.786	0.374
all-UnityEyes	0.625	0.279		0.385	0.580	0.949	0.427	1.675	0.274
all-RI TEyes-Gen	0.659	0.326		0.692	0.778	1.062	0.622	1.789	0.323
all-RI TEyes-Nat	0.598	0.283		0.503	1.003	0.936	0.439	1.763	0.265
all-LPW	0.661	0.293		0.542	0.756	1.550	0.484	1.707	0.414
all-Santini	0.606	0.265		0.343	0.515	0.896	1.543	1.689	0.250
all-Fuhl	0.597	0.272		0.414	0.579	0.920	0.500	2.627	0.347
all-Swirski	0.660	0.256		0.363	0.528	0.988	0.410	1.712	0.980
all	0.669	0.272		0.461	0.642	1.085	0.691	1.842	0.463

Table 3. Error in pupil center prediction across various generalization tests proposed in Section 3.4. All results are presented in unit pixels.

Train on / Test on	OpenEDS	NVGaze	UnityEyes	RTEyes-Gen	RTEyes-Nat	LPW	BAT	Fuhl	Swirski
OpenEDS	1.848	5.864	11.039	14.375	31.254				
NVGaze	4.249	0.300	9.760	15.680	31.174				
UnityEyes	7.438	3.458	0.651	9.790	16.928				
RTEyes-Gen	3.885	2.749	4.047	0.702	1.099				
RTEyes-Nat	4.404	2.741	2.413	0.618	0.610				
LPW									
BAT									
Fuhl									
Swirski									
all-OpenEDS	4.225	0.353	1.364	0.581	0.715				
all-NVGaze	1.860	2.731	1.643	0.721	0.853				
all-UnityEyes	1.903	0.367	3.582	0.663	0.800				
all-RTEyes-Gen	2.060	0.462	1.697	0.997	1.064				
all-RTEyes-Nat	2.121	0.430	1.928	0.893	1.513				
all-LPW	2.097	0.413	1.501	0.716	0.874				
all-BAT	1.858	0.399	1.430	0.698	0.829				
all-Fuhl	2.037	0.405	1.620	0.645	0.783				
all-Swirski	1.856	0.441	1.427	0.689	0.822				
all	2.171	0.441	1.460	0.883	1.033				

Table 4. Error in iris center prediction across various generalization tests proposed in Section 3.4. All results are presented in unit pixels.

Train on / Test on	OpenEDS	NVGaze	UnityEyes	RTEyes-Gen	RTEyes-Nat	LPW	BAT	Fuhl	Swirski					
OpenEDS	0.956	0.572		0.550	0.427									
NVGaze	0.664	0.986		0.570	0.355									
UnityEyes														
RTEyes-Gen	0.713	0.883		0.960	0.932									
RTEyes-Nat	0.812	0.917		0.954	0.948									
LPW														
Santini														
Fuhl														
Swirski														
all-OpenEDS	0.688	0.486		0.822	0.850									
all-NVGaze	0.920	0.428		0.729	0.757									
all-UnityEyes	0.949	0.950		0.950	0.937									
all-RTEyes-Gen	0.933	0.442		0.685	0.787									
all-RTEyes-Nat	0.939	0.466		0.802	0.698									
all-LPW	0.952	0.967		0.954	0.942									
all-Santini	0.952	0.963		0.957	0.946									
all-Fuhl	0.949	0.958		0.955	0.943									
all-Swirski	0.950	0.954		0.952	0.940									
all	0.956	0.982		0.961	0.947									

Table 5. Segmentation results of various generalization tests proposed in Section 3.4 when utilizing Batch Normalization. All results represent the IoU metric.

Train on / Test on	OpenEDS	NVGaze	UnityEyes	RITEyes-Gen	RITEyes-Nat	LPW	BAT	Fuhl	Swirski
OpenEDS	0.614	2.102		8.346	18.620	1.349	1.951	4.920	1.583
NVGaze	1.031	0.201		13.952	61.093	4.483	2.139	67.145	4.146
UnityEyes									
RITEyes-Gen	0.732	1.262		0.302	0.720	1.735	2.375	32.363	1.160
RITEyes-Nat	0.801	0.681		0.355	0.481	1.581	2.243	6.457	2.001
LPW	0.737	1.448		3.205	8.256	0.638	1.694	5.471	1.022
Santini	1.740	1.838		3.256	4.458	2.634	0.494	3.994	1.633
Fuhl	1.313	1.796		3.469	5.272	2.696	1.045	1.724	1.740
Swirski	2.003	2.723		3.818	5.200	4.189	0.747	7.593	0.616
all-OpenEDS	1.387	0.637		0.717	0.924	1.260	0.688	1.771	0.437
all-NVGaze	1.088	1.196		0.767	0.897	1.089	0.585	2.060	0.704
all-UnityEyes	1.091	0.660		0.544	0.674	0.826	0.529	1.798	0.392
all-RITEyes-Gen	1.614	0.820		0.957	1.051	1.166	0.492	1.701	0.447
all-RITEyes-Nat	1.242	0.725		0.786	1.213	0.986	0.623	1.918	0.530
all-LPW	1.071	0.353		0.462	0.600	1.310	0.419	1.718	0.265
all-Santini	0.829	0.306		0.499	0.657	0.822	1.390	1.937	0.328
all-Fuhl	0.823	0.369		0.487	0.643	0.791	0.748	2.374	0.448
all-Swirski	1.113	0.491		0.435	0.577	0.855	0.478	1.777	0.533
all	1.190	0.645		0.673	0.835	1.156	0.934	1.915	0.732

Table 6. Error in pupil center prediction across various generalization tests proposed in Section 3.4 when utilizing Batch Normalization. All results are presented in unit pixels.

Train on / Test on	OpenEDS	NVGaze	UnityEyes	RI TEyes-Gen	RI TEyes-Nat	LPW	BAT	Fuhl	Swirski
OpenEDS	1.782	5.021	27.025	21.102	31.861				
NVGaze	5.354	0.268	14.095	16.955	44.660				
UnityEyes	4.629	2.340	0.807	2.251	2.988				
RI TEyes-Gen	4.568	2.687	10.048	0.598	0.928				
RI TEyes-Nat	4.861	2.564	5.654	0.743	0.756				
LPW									
BAT									
Fuhl									
Swirski									
all-OpenEDS	3.823	1.610	1.920	1.111	1.268				
all-NVGaze	2.828	2.999	2.161	1.036	1.124				
all-UnityEyes	2.381	1.526	3.848	1.181	1.293				
all-RI TEyes-Gen	2.793	1.789	1.782	1.074	1.140				
all-RI TEyes-Nat	2.824	2.255	1.687	1.086	1.476				
all-LPW	2.347	0.763	1.774	0.879	0.982				
all-BAT	2.603	0.987	2.286	1.026	1.158				
all-Fuhl	2.721	0.847	2.047	0.858	0.957				
all-Swirski	2.301	1.092	2.241	1.034	1.115				
all	2.171	0.441	1.460	0.883	1.033				

Table 7. Error in iris center prediction across various generalization tests proposed in Section 3.4 when utilizing Batch Normalization. All results are presented in unit pixels.

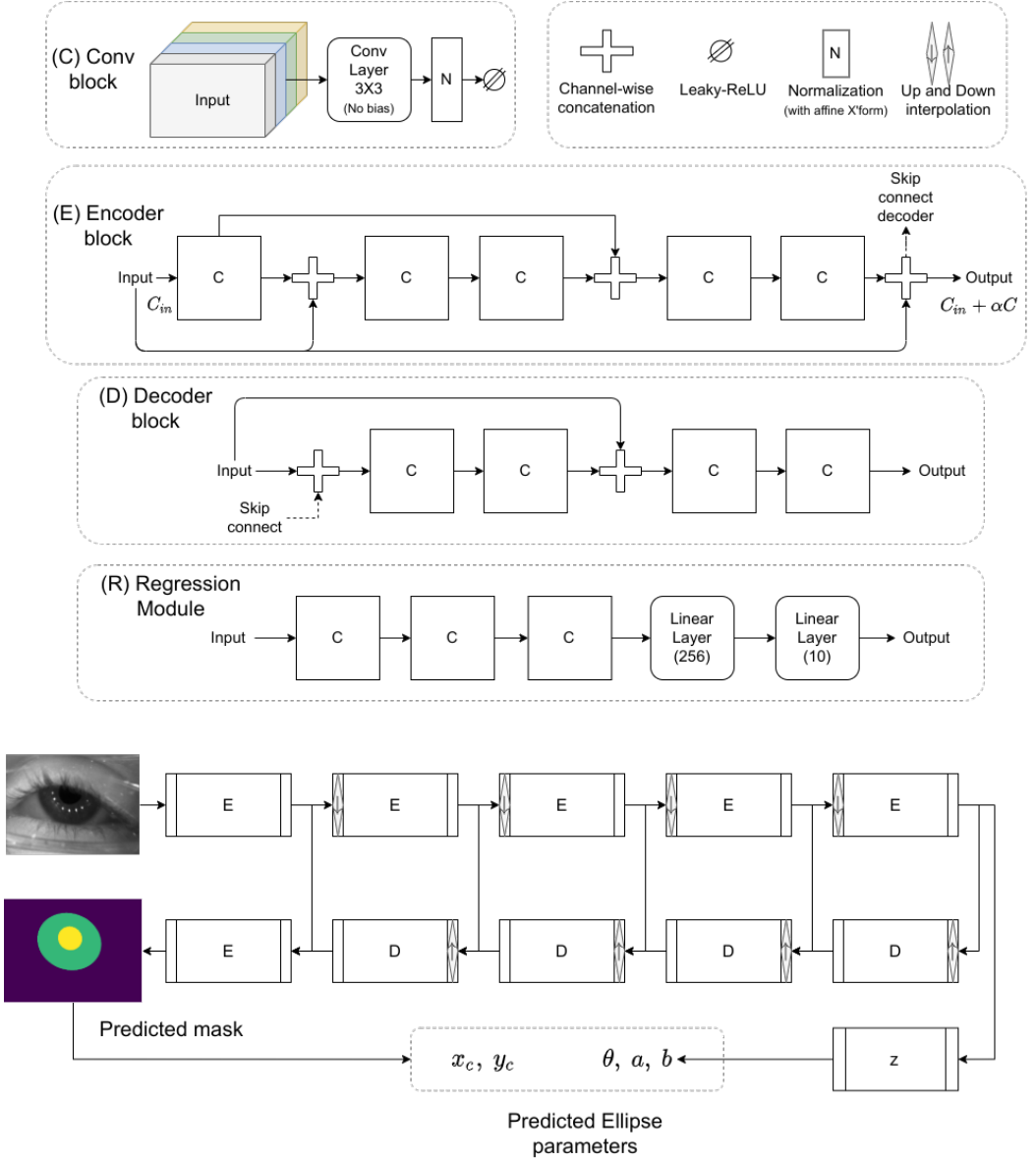


Fig. 1. DenseEINet architecture adapted from EIIseg. The number of parameters in the encoder are controlled by a base channel size of C and a growth rate of α .

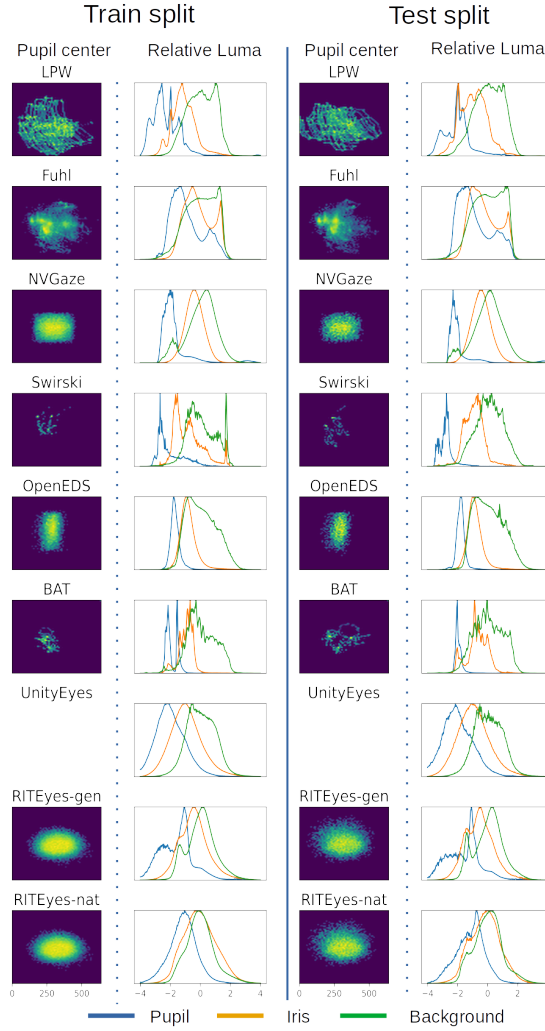
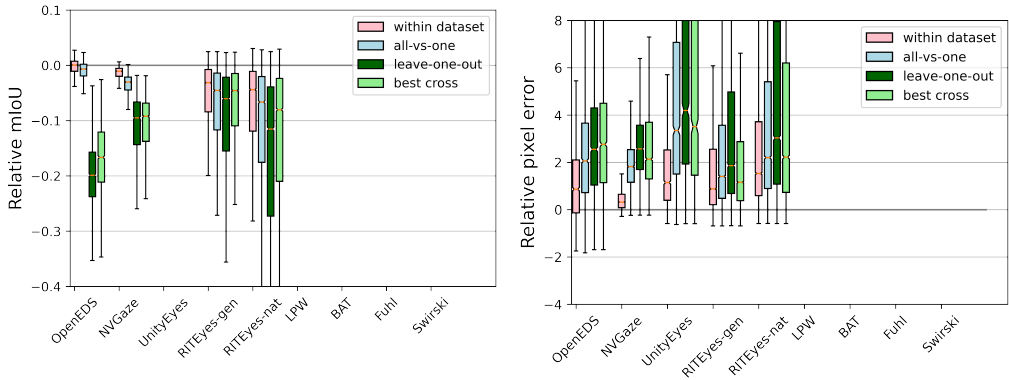
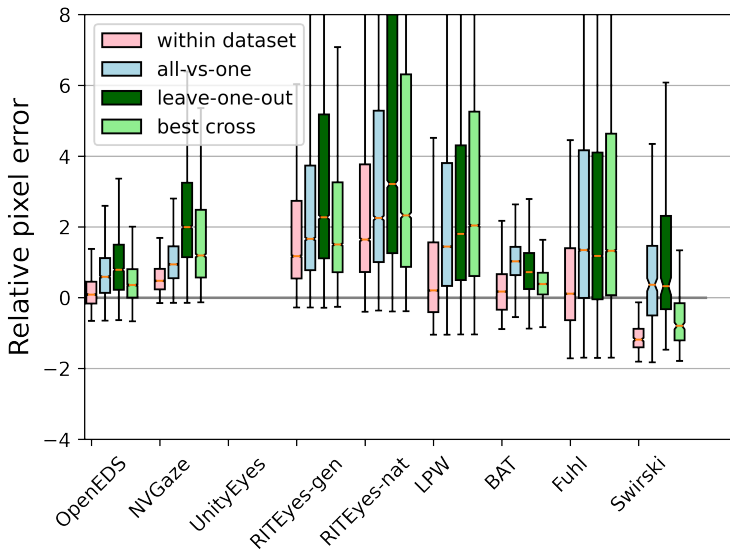


Fig. 2. Pupil center (in pixels) and normalized luminance distribution (in Z-scores) of each eye part across all datasets utilized in our experiments (see Table 1). The left and right columns contain statistics from the training and test images for each domain respectively. Due to partial annotations present in some datasets, we leverage the all-vs-one model predictions to segment eye images from all datasets into pupil, iris and background segments. Luminance statistics are then accumulated from the predicted segmentation map.



(a) Performance following reduction in network complexity measured as the mIoU metric relative to training in the absence of augmentation. Positive values indicate a performance improvement.

(b) Performance following reduction in network complexity measured as error in iris center, e_i , in pixels. Negative values indicate a performance improvement.



(c) Performance following reduction in network complexity measured as error in pupil center e_p in pixels. Negative values indicate a performance improvement.

Fig. 3. The effect of reducing model complexity from 2.2M to 529K parameters. This is achieved by setting the growth factor to 1 and increasing the number of grouped filters to 32 per convolution layer. Each box plot highlights a model's performance centered to the within-dataset limit for each domain. The line and notch present within each box plot represents the median and confidence interval respectively while the ends of each box denotes the 1st and 3rd quartile. All images are 320×240 resolution. Note that boxplots pertaining to datasets without a certain groundtruth annotation are missing. All measures are centered to the within-dataset threshold as reported in Figure 2 and Supplementary Tables 2, 3 and 4